

A MULTITASK DEEP LEARNING MODEL FOR PARSING BRIDGE ELEMENTS AND SEGMENTING DEFECT IN BRIDGE INSPECTION IMAGES

Chenyu Zhang

Department of Civil Engineering, Stony Brook University
Stony Brook, NY 11794
chenyu.zhang.1@stonybrook.edu

Muhammad Monjurul Karim

Department of Civil Engineering, Stony Brook University
Stony Brook, NY 11794
muhammadmonjur.karim@stonybrook.edu

Ruwen Qin

Department of Civil Engineering, Stony Brook University
Stony Brook, NY 11794
ruwen.qin@stonybrook.edu

Word Count: 5281 words + 5 tables \times 250 = 6531 words

Submission Date: August 1, 2022

ABSTRACT

The vast network of bridges in the United States raises a high requirement for its maintenance and rehabilitation. The massive cost of manual visual inspection to assess the conditions of the bridges turns out to be a burden to some extent. Advanced robots have been leveraged to automate inspection data collection. Automating the segmentations of multiclass elements, as well as surface defects on the elements, in the large volume of inspection image data would facilitate an efficient and effective assessment of the bridge condition. Training separate single-task networks for element parsing (i.e., semantic segmentation of multiclass elements) and defect segmentation fails to incorporate the close connection between these two tasks in the inspection images where both recognizable structural elements and apparent surface defects are present. This paper is motivated to develop a multitask deep neural network that fully utilizes such interdependence between bridge elements and defects to boost the performance and generalization of the model. Furthermore, the effectiveness of the proposed network designs in improving the task performance was investigated, including feature decomposition, cross-talk sharing, and multi-objective loss function. A dataset with pixel-level labels of bridge elements and corrosion was developed for training and assessment of the models. Quantitative and qualitative results from evaluating the developed multitask deep neural network demonstrate that the recommended network outperforms the independent single-task networks not only in performance (2.59% higher mIoU on bridge parsing and 1.65% on corrosion segmentation) but also in computational time and implementation capability.

Keywords: Infrastructure condition assessment, Bridge inspection, Multitask learning, Multiclass segmentation, Computer vision

INTRODUCTION

The United States has 619,588 bridges in its inventory, and 36% need replacement or rehabilitation (1). As the average age of the bridges has increased to 44 years, the cumulative effects of structure loading, environment, and deferred maintenance will deteriorate structural elements progressively (2). Bridges in the U.S. are evaluated periodically to determine whether deterioration has occurred, which requires follow-up corrective actions. The conventional manual bridge inspection is still the main form of assessing civil infrastructure conditions (3). Limitations of the traditional approach motivate research into automating bridge inspection and monitoring using emerging technologies such as robotics and artificial intelligence. It is an inevitable step forward and can be readily adapted to aid and eventually replace the manual inspection while offering new advantages and opportunities.

Mobile robots, such as unmanned aerial vehicles (UAVs), are cost-effective tools for gathering inspection video or image data (4). They reduce the time, labor, and equipment costs of the onsite inspection process. To make the most of robotic inspection platforms and automation of the inspection process, efficient and dependable methods to analyze inspection data are required. For example, a real-time assessment of the bridge condition based on RGB camera sensors would help prioritize the data collection by other sensors that are in high resolution but more time-consuming and energy-consuming. The Bridge Element Inspection Manual published by the American Association of State Highway and Transportation Officials (AASHTO) (5) states that an overall condition rating of a bridge is based on a comprehensive assessment that relates the defects to specific structural elements. Therefore, extracting or detecting bridge elements and their defects from collected image data is essential.

Detecting and segmenting defects on civil structures is an area of research interest in structural health monitoring. The rapid development of graphics processing units and deep learning algorithms have significantly advanced computer vision-based defect analysis. Researchers have achieved impressive results in identifying various damage or defect types, such as concrete crack, steel crack, asphalt crack, spalling, steel corrosion, exposed rebar, and many others (6). However, many models are trained on images that primarily contain pixel-level details of surface defects and can be called defect-level images as shown in FIGURE 1(a). Those images are relatively easy to analyze because defects are in a closer look, and the background is greatly homogeneous. Defect-level images must be either taken from a position closer to defects or pre-processed (i.e., cropped and zoomed in), which raises higher requirements for the operators of UAVs or increases the workload of image analysis.



(a) Defect-level



(b) Structure-level



(b) Combined-level

FIGURE 1: Different Levels of Inspection Images

Compared to the large volume of studies on defect detection and segmentation, research on extracting multiclass structural elements from inspection images or videos is limited and remains challenging (7–10). Prior work used structure-level images where multiple elements of a civil structure are salient objects as shown in FIGURE 1(b). In these images, many elements and components are distinguishable, but the detailed information on the element surface is missing.

Nevertheless, cameras also capture bridge images from a certain distance where images have recognizable structural elements and apparent surface defects on the elements as shown in FIGURE 1(c). Combined-level inspection images like such provide valuable information for a quick, automatic assessment of the bridge condition. In those images, bridge elements of the same type have widely different appearances due to the imperfect and changing view of the mobile cameras. Due to the typically irregular shape of bridge elements and defects, semantic segmentation is more suitable than other identification approaches for parsing inspection images. To our best knowledge, this kind of inspection images and the association between bridge elements and their defects have not been fully utilized and studied yet.

A naive way to analyze bridge elements and defects in combined-level images is to train separate networks for the two tasks. Yet, this approach ignores the relationship between these two tasks. It is likely to obtain low generalizability and learn similar features resulting in inefficient use of information-sharing, computation resources, and network capability. Attempts to improve the performance of element and defect segmentation have mainly focused on refining network architectures (deeper and broader) and increasing training data. Instead, an efficient approach would be multitask learning (MTL), meaning that learning multiple tasks simultaneously through optimizing more than one loss function in a single model. An MTL model learns generalized representations of the data, which are useful in multiple contexts. Besides improved learning efficiency and prediction accuracy, MTL can reduce the risk of overfitting.

The task of structural element parsing involves extracting structural elements of bridges and classifying them. The defect segmentation task is to assign a defect label for each pixel. Structural element parsing and defect segmentation are two correlated tasks. For example, corrosion can be developed on elements made with metals, but not concrete, masonry, and composite materials. This correlation has not been fully utilized and studied yet. Given the hypothesis that related tasks may benefit from MTL, this paper proposes a multitask deep learning model to parse multiclass bridge elements and segment defects simultaneously. Alignment of the two tasks' outputs from the multitasking model is convenient and allows locating both defective elements in images and the defects on those elements easily.

The rest of the paper is organized as follows. The next section summarizes the related work. Then, the following section introduces the proposed MTL network and evaluation metrics. After that, the dataset and implementation details are delineated, followed by a qualitative and quantitative analysis of the results. Finally, the conclusion and future work are summarized.

LITERATURE REVIEW

Computer Vision-based Structural Defect Detection and Segmentation

Prior studies have mainly concentrated on locating concrete cracks using conventional image processing methods. Restricted to their computational cost and limited performance, these traditional algorithms can only identify defects with specific patterns and can not utilize contextual information in inspection images. The performance of machine learning on defect detection improved significantly as the popularity of convolutional neural networks (CNNs) (11). The high-resolution

network (HRNet) (12) is a general-purpose CNN that can maintain high-resolution representations through the whole process by connecting high-to-low resolution convolutions in parallel. It has been successfully applied to the surface defect detection and segmentation (13–15).

Especially, defect segmentation can be divided into semantic segmentation and instance segmentation. Semantic segmentation is a per-pixel classification task that does not differentiate different objects in the same class. Rubio et al. (16) and Dung et al. (17) applied fully convolutional network (FCN) to complete semantic segmentation for bridge deck damages (delamination and rebar exposure) and concrete cracks, respectively. Based on the U-Net (18) and attention mechanism, Pan et al. (19) proposed PipeUNet to segment sewer defects (crack, infiltration, joint offset, and intruding lateral). Wang and Cheng (20) proposed DilaSeg-CRF for segmenting sewer pipe defects (crack, deposit, and root) based on PSPNet (21). Shi et al. (22) conducted damage segmentation of steel corrosion and rubber bearing crack by U-Net. Instance segmentation can be a combined task of semantic segmentation and object detection, which differentiates different objects in the same class. Mask R-CNN was successfully utilized for concrete bridge cracks segmentation (23), façade defects segmentation (24), and shield tunnel lining cracks segmentation (25).

Structural Element Detection and Segmentation

Element detection and segmentation is an indispensable part of automated bridge inspection, yet it does not step forward to a promising level. Extracting bridge elements from inspection images is still not completely solved due to its higher complexity than the defect detection and segmentation task and the insufficient inspection dataset.

Yeum et al. (26) developed a CNN-based method to extract the regions of interest on inspection images for visual evaluation. Narazaki et al. (7) trained a scene classifier to segment five bridge components. Bianchi et al. (8) applied the SSD v2 model (27) to achieve bridge details detection and investigated the use of image augmentation to boost the performance of the trained model. Karim et al. (9) transferred a Mask R-CNN pre-trained on a large public dataset to segment multiclass bridge elements. They also developed a semi-supervised self-training method to engage the inspector to refine the network iteratively. Zhang et al. (10) demonstrated that HRNetV2-W32 is a suitable network for segmenting multiclass structural elements from bridge inspection images through a comparison with the state-of-the-art semantic segmentation networks.

Multitask Learning

Multitask learning (MTL) has been successfully used in many tasks of computer vision, such as depth estimation and surface normal prediction (28), segmentation of building footprints (29), pedestrian detection (30), and facial landmark detection (31), and so on. The most commonly used way to achieve MTL is to share feature extractor and branch down-stream tasks for task-wise predictions (32). The shared feature extractor learns common representations for all tasks, which can dramatically lower the risk of overfitting and improve generalization (33). Hoskere et al. (34) proposed a deep neural network MaDnet composed of multiple semantic segmentation paths with a shared feature extractor to identify material and damage types. This framework suggests useful contextual information exists in basic automated inspection tasks and can be helpful to them. For the bridge element and defect segmentation tasks, one can be an auxiliary task to another and help another by introducing more annotations and perspectives.

METHODOLOGY

FIGURE 2 illustrates the architecture of the MTL model. The input is an RGB image of height H and width W . First, the shared feature extractor extracts and generates the common feature embedding, $\mathbf{F}(\in \mathbb{R}^{c \times h \times w})$, from the input image, where c is the number of feature maps, and h and w are the height and width of the feature maps. Then, \mathbf{F} flows into two branches that are respectively dedicated to the two tasks: element parsing and defect segmentation.

In the element parsing branch, a projection network extracts the element-specific feature embedding, $\mathbf{f}_e(\in \mathbb{R}^{c \times h \times w})$, from the common feature embedding. \mathbf{f}_e is input to the element parsing network to become a downsampled feature embedding, $\mathbf{O}_e(\in \mathbb{R}^{c_e \times h \times w})$, with the number of channels equal to the number of element classes, c_e . \mathbf{O}_e is further upsampled to get the element prediction, $\hat{\mathbf{y}}_e(\in \mathbb{R}^{c_e \times H \times W})$. The branch of the defect segmentation is similarly defined.

The output from the defect segmentation network, $\mathbf{O}_d(\in \mathbb{R}^{c_d \times h \times w})$, can be concatenated with the element-specific feature embedding \mathbf{f}_e to provide the defect awareness to the element parsing task. Similarly, \mathbf{O}_e can provide the element awareness to the defect segmentation task. This is termed cross-talk sharing. The dashed lines in FIGURE 2 represent this design, which will be evaluated in the result section.

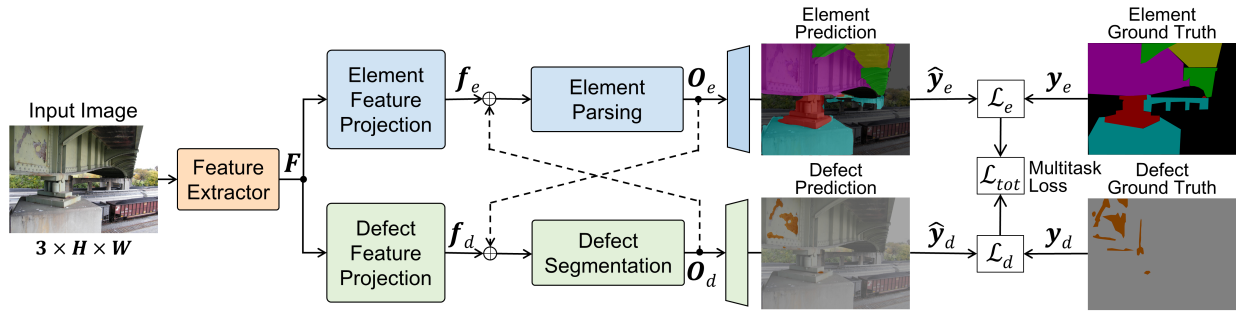


FIGURE 2: Architecture of the Multitask Deep Learning Model

Feature Extraction

This study uses the backbone HRNetV2-W32 to extract features from input images. Semantic segmentation is a highly position-sensitive task that needs spatially-fine representation. HRNet is selected for this study since this network has the ability to learn weak position-sensitivity of the representation. HRNetV2-W32 takes the input image and maps it into a dense embedding \mathbf{F} . In this study, the dimension of input images are $3 \times 480 \times 480$ (i.e., $H = W = 480$). The common feature embedding \mathbf{F} of input images contains 480 feature maps in size 120×120 (i.e., $c = 480$, and $h = w = 120$).

Feature Decomposition

The common feature embedding of an input image, \mathbf{F} , contains both element-related information and defect-related information. The element-specific features, \mathbf{f}_e , and the defect-specific features, \mathbf{f}_d , intertwined in \mathbf{F} are decomposed using two projection modules:

$$\begin{aligned} \mathbf{f}_e &= P(\mathbf{F}; \Phi_e, \beta_e), \\ \mathbf{f}_d &= P(\mathbf{F}; \Phi_d, \beta_d). \end{aligned} \tag{1}$$

where $P(\mathbf{F}; \Phi, \beta)$ represents a projection network that maps the input feature map \mathbf{F} onto a new space in the same dimension using the projection matrix $\Phi (\in \mathbb{R}^{c \times c})$ and the bias vector $\beta (\in \mathbb{R}^{c \times 1})$. However, the projection network can have different designs. For example, When both Φ and β are scalars, the projection is simply about scaling the input embedding linearly and then shifting it to become the task-related feature embedding. When the projection parameters are vectors in the same dimension as the input embedding's feature map numbers (c), the projection is about adding the channel-wise attention to \mathbf{F} . The result section will evaluate the performance of the different projection designs.

Segmentation Networks

In each branch, one convolutional network is used to downsample the feature embedding \mathbf{f} to become \mathbf{O} . The information flow for both the branches can be represented as:

$$\begin{aligned} \mathbf{O}_e &= \text{Conv}(\text{Conv}(\text{Cat}(\mathbf{f}_e, \mathbf{O}_d); \boldsymbol{\theta}_{e1}); \boldsymbol{\theta}_{e2}) \\ \mathbf{O}_d &= \text{Conv}(\text{Conv}(\text{Cat}(\mathbf{f}_d, \mathbf{O}_e); \boldsymbol{\theta}_{d1}); \boldsymbol{\theta}_{d2}) \end{aligned} \quad (2)$$

where $\text{Cat}(\cdot, \cdot)$ means the concatenation operation, $\text{Conv}(\cdot; \boldsymbol{\theta})$ means convolution operation with learnable parameters $\boldsymbol{\theta}$. In this study, $\mathbf{O}_e \in \mathbb{R}^{7 \times 120 \times 120}$ (i.e., $c_e = 7$) since the element parsing task has 7 classes including the background class. $\mathbf{O}_d \in \mathbb{R}^{2 \times 120 \times 120}$ (i.e., $c_d = 2$) because the defect segmentation has only two classes (corrosion vs. no corrosion).

The downsampled feature embeddings, \mathbf{O}_e and \mathbf{O}_d , are projected into two separate score maps to get the element and defect predictions, $\hat{\mathbf{y}}_e$ and $\hat{\mathbf{y}}_d$, respectively:

$$\begin{aligned} \hat{\mathbf{y}}_e &= S(\mathbf{O}_e; \boldsymbol{\varphi}_e) \\ \hat{\mathbf{y}}_d &= S(\mathbf{O}_d; \boldsymbol{\varphi}_d) \end{aligned} \quad (3)$$

where $S(\cdot; \boldsymbol{\varphi})$ represents the mapping function with learnable parameters $\boldsymbol{\varphi}$ that upsamples the output maps to become the same size as the input images. This mapping function upsamples the output score maps to become the same size of the input image's label maps. That is, $\hat{\mathbf{y}}_e \in \mathbb{R}^{7 \times 480 \times 480}$ and $\hat{\mathbf{y}}_d \in \mathbb{R}^{2 \times 480 \times 480}$.

The Loss Function

The cross-entropy loss for the element parsing task, \mathcal{L}_e , and that for the defect segmentation task, \mathcal{L}_d , are calculated:

$$\begin{aligned} \mathcal{L}_e &= - \sum_k \langle \mathbf{y}_e(k), \log \hat{\mathbf{y}}_e(k) \rangle, \\ \mathcal{L}_d &= - \sum_k \langle \mathbf{y}_d(k), \log \hat{\mathbf{y}}_d(k) \rangle, \end{aligned} \quad (4)$$

where k is the index of images in the training dataset, $\mathbf{y}(k)$ and $\hat{\mathbf{y}}(k)$ are the ground-truth and prediction of the k th training image, and $\langle \cdot, \cdot \rangle$ is the Frobenius inner product.

The respective loss functions of the two tasks are combined as the multitask loss function, \mathcal{L}_{tot} . The performance of MTL strongly depends on the relative weights between each task's loss (35). Manually tuning these weights is difficult and costly, making MTL prohibitive in practice. The easiest way is just to take equal weights for both tasks, $\mathcal{L}_e + \mathcal{L}_d$, called the additive loss function.

Therefore, developing a more practical method to determine the optimal weights would be ideal. One approach considered in this study is to use the homoscedastic uncertainty of each task

(36) to weight its loss:

$$\mathcal{L}_{tot} = \frac{1}{2\sigma_e^2} \mathcal{L}_e + \frac{1}{2\sigma_d^2} \mathcal{L}_d + \log \sigma_e \sigma_d, \quad (5)$$

where σ_e and σ_d are noise parameters for the two tasks, respectively. They are learnable weights for the minimization objective. Both the additive and homoscedastic uncertainty loss functions are examined in the result section.

Evaluation Metrics

To evaluate the performance of the two tasks, four metrics are calculated at the class level of each task:

$$\text{Precision} = \frac{\text{No. correctly predicted pixels}}{\text{No. pixels predicted to be the class}} \quad (6)$$

$$\text{Recall} = \frac{\text{No. correctly predicted pixels}}{\text{No. pixels of the class}} \quad (7)$$

$$\text{F1} = \frac{2 \times \text{Precision} \times \text{Recall}}{\text{Precision} + \text{Recall}} \quad (8)$$

$$\text{IoU} = \frac{\text{No. pixels common between the ground-truth and prediction masks}}{\text{No. pixels present across both masks}} \quad (9)$$

where IoU stands for Intersection over Union.

Then, the average values across classes are further calculated, including mean Precision (mPrecision), mean Recall (mRecall), mean F1-score (mF1), and mean IoU (mIoU), to obtain the task-level performance metrics.

DATASET AND IMPLEMENTATION

The proposed MTL networks require labeled datasets for training and testing. This section illustrates the dataset developed for the proposed networks and the implementation details of the models.

The Dataset

As one of the most common types of bridges in the U.S., steel bridges are susceptible to atmospheric corrosion. Deck runoff and traffic-generated aerosols that contain deicing salts can accelerate corrosion. General corrosion may result in loss-of-section of bridge components, greater dead, live stresses, and stress concentrators, which might lead to cracking issues in the future. Today, general corrosion on steel bridges is perhaps the most prevalent issue.

The study covered 145 images, a portion of the Corrosion Condition State Semantic Segmentation Dataset (37). The inspection images were collected from the Virginia Department of Transportation Bridge Inspection Reports and semantically annotated following the corrosion condition state guidelines stated in the Bridge Inspector's Reference Manual (5).

This project used the image annotation tool LabelMe (38) to provide the pixel-level annotation of six common classes of structural elements for steel girder bridges in these inspection images: Bearing (Brg), Bracing (Brc), Deck (Dck), Floor beam (Flb), Girder (Grd), and Substructure (Sbt). In total, 822 instances are annotated in the 145 images. Also, the study converted the annotation of the original four corrosion class categories: Good, Fair, Poor, and Severe, into the

annotation of binary corrosion class categories: Corrosion (Cor) and No Corrosion (No), for the MTL model. The study reserves 130 images for training models and 15 images for testing. TABLE 1 further summarizes the distribution of element instances and the pixel proportion of defect areas (% defect area) in the training and testing subset. The structural element proportions range from 10% to 29% and are all above 10%, and the defect area proportions are about 2:8, which reflects the actual bridge inspection situation and is eligible for training.

TABLE 1: Distribution of the Structural Elements and Defect

	No. images	No. structural elements						% defect area	
		Brg	Brc	Dck	Flb	Grd	Sbt	Cor	No
Training	130	169	76	104	84	217	99	17.3	82.7
Testing	15	19	6	6	10	20	12	13.9	86.1
Total	145	188	82	110	94	237	111	16.9	83.1
Proportion (%)		23	10	13	11	29	14		

Model Training

The backbone HRNetV2-W32 in this study was initialized by adopting the weights pre-trained on the PASCAL Visual Object Classes (VOC) 2012 dataset and Semantic Boundaries Dataset (SBD). Then, transfer learning was used to adapt the backbone to the two semantic segmentation tasks. Training and testing were performed using one Nvidia Tesla V100 GPU with 32 GB of memory. All images were resized from the original size to 480×480 (i.e., $H = W = 480$). This study employed data augmentation techniques to increase the diversity and representation of the training dataset, thus improving the network's generalization ability. Specifically, random scale transformation was conducted together with geometric distortion, random rotations between $\pm 10^\circ$ and, random horizontal flipping, random image intensity noise using 5×5 Gaussian kernel, and HSV augmentation. The optimizer Adam was used for training models. The schedule applies an exponential decay function to the optimization step, given a provided initial learning rate of 5e-4 and the minimum of 5e-6. A batch size of 8 was used in this training process.

EXPERIMENTS AND RESULTS

This section compares the proposed MTL models of different designs with individual single-task networks and describes the results and discussions from the conducted experiments.

Design of Experiments

To illustrate the superiority of the MTL model, three single-task HRNetV2 models were trained, where each is composed of the backbone of HRNet and a segmentation head. The first two single-task networks were trained for the bridge element parsing and the defect segmentation, respectively. The third network (merged-task) combines element and defect labels and defines bridge element classes as elements with defects and without defects. To fully examine and boost the potential and performance of MTL, this study develops twelve different versions of the MTL model as shown in TABLE 2. Firstly, three kinds of projection method were proposed and examined: scalar, vector, and matrix. The effect of cross-talk sharing (i.e., the dashed lines in FIGURE 2)

between the MTL model’s two branches was explored. Two different loss functions, the additive loss and the homoscedastic uncertainty loss, were compared.

TABLE 2: Different Versions of Multitask Deep Learning Model

Index	Projection	Cross-talk	Loss function
MTL-A	Scalar	No	Additive
MTL-B	Scalar	No	Homoscedastic uncertainty
MTL-C	Scalar	Yes	Additive
MTL-D	Scalar	Yes	Homoscedastic uncertainty
MTL-E	Vector	No	Additive
MTL-F	Vector	No	Homoscedastic uncertainty
MTL-G	Vector	Yes	Additive
MTL-H	Vector	Yes	Homoscedastic uncertainty
MTL-I	Matrix	No	Additive
MTL-J	Matrix	No	Homoscedastic uncertainty
MTL-K	Matrix	Yes	Additive
MTL-L	Matrix	Yes	Homoscedastic uncertainty

Performance Comparison

The results from the twelve versions of the MTL model are compared against the results from the single-task networks as shown in TABLE 3. Below findings can be drawn from the performance comparison. The two independent single-task networks achieved fine results on these two tasks with limited training data. The merged-class single-task network achieved comparable results to the single-task network on the element parsing task. However, for corrosion segmentation task, its performance dropped by 27.12% on mIoU, 12.92% on mPrecision, 28.83% on mRecall, and 21.39% on mF1. Because the elements with and without corrosion both lose their shape and position features. It is hard to classify the corrosion for the model, resulting in decreased corrosion segmentation task results. Overall, the merged-class single-task network is unsuitable for these two tasks, although it can simultaneously complete two tasks using a single-task architecture.

The proposed MTL models outperformed the single-task and the combined-class single-task networks for all the performance metrics of the two tasks except the mRecall of corrosion segmentation task. The improvement in mIoU of the bridge parsing task due to the introduction of MTL ranges from 0.78% to 2.59%, and 0.55% to 2.46% for the corrosion segmentation task with the same training data and hyperparameters. The MTL-I model is the best in terms of mIoU, mRecall, and mF1 on the bridge parsing task. MTL-D is the best in terms of mIoU and mF1 on the corrosion segmentation task. These two models will be further discussed and compared in the following.

For the projection method, as the complexity increases from a scalar to a matrix, there is no clear improvement. The potential reason could be that more complexity means more difficult for training and optimization. Then, for the cross-talk sharing between the two tasks, the networks were improved, particularly on the corrosion segmentation task. The highest increase on mIoU was 1.21% between MTL-C and MTL-A for the corrosion task. Last but not least, the modification of

the loss function matters in MTL. The MTL models using the scalar projection benefit from the homoscedastic uncertainty weight, as well as the networks using the vector projection without cross-talk. The improvements were not remarkable for the networks using the vector projection with cross-talk and the matrix projection as they have too high complexity to optimize with limited training data. But the performance of complex models could be further improved if increasing the size of training dataset.

TABLE 3: Performance Comparison Between Single- and Multi-task Networks

Network	Bridge Parsing Task				Corrosion Segmentation Task			
	mIoU	mPrecision	mRecall	mF1	mIoU	mPrecision	mRecall	mF1
Single-task	82.89	90.75	90.41	90.58	80.85	87.20	90.76	88.94
Merged-task	82.35	90.17	90.39	90.28	53.73	74.28	61.93	67.55
MTL-A	85.10	92.34	91.40	91.88	81.40	88.78	89.74	89.26
MTL-B	84.38	91.74	91.14	91.44	83.15	90.58	90.14	90.36
MTL-C	83.67	91.87	90.37	91.11	82.61	89.47	90.58	90.02
MTL-D	84.41	92.01	91.04	91.52	83.31	90.09	90.85	90.47
MTL-E	84.39	91.36	91.74	91.55	82.78	89.39	90.90	90.14
MTL-F	84.66	91.63	91.60	91.61	82.93	90.01	90.43	90.22
MTL-G	85.00	91.51	92.13	91.82	82.26	89.04	90.57	89.80
MTL-H	84.82	91.37	92.09	91.73	81.91	88.66	90.51	89.58
MTL-I	85.48	92.00	92.33	92.16	82.50	89.74	90.13	89.93
MTL-J	83.74	91.63	90.56	91.09	81.88	88.90	90.20	89.55
MTL-K	84.63	92.12	91.11	91.61	82.79	89.94	90.31	90.12
MTL-L	83.79	91.25	90.90	91.07	82.31	89.49	90.13	89.81

The highest value for each index among all networks is shown in bold text

Performance Comparison by Class

To better illustrate the performance improvement on each class by the introduction of MTL, the two MTL networks, MTL-D and MTL-I, performed the best in terms of mIoU on the bridge element parsing task and defect segmentation task, respectively were selected to have a close look as shown in TABLE 4. The single-task networks are taken as the benchmark for comparison.

For the bridge element parsing task, the MTL-I model has a noticeable performance improvement compared to the single-task network. It significantly outperforms the single-task network on IoU, particularly for bracing and deck with more than 5% improvement (6.42% for bracing and 5.02% for deck). For substructure and background, the increases in IoU are more than 2%, which is also inspiring (2.64% for substructure and 2.40% for background). For the IoU of segmenting bearing, floor beam, and girder classes, MTL-I still achieved better results, although the improvements are limited to 1% (0.27% for bearing, 0.84% for floor beam, and 0.58% for girder). On precision, the MTL-I network broadly achieves better results on each class except for bracing, ranging from 0.45% on the girder class to 3.61% on the floor beam class. On recall, the improvement by the MTL-I network can be seen in each class apart from bearing and floor beam classes, and especially for bracing, the progress reached surprisingly 10.60%. The introduction of

defect features provides more information to the model and reinforce the network's segmentation capability on the edges of elements, therefore improve the MTL models' performance on element parsing task.

For the defect segmentation task, the MTL-D network also shows a dominant performance to the single-task network. On IoU, the improvements of the MTL-D network are 3.78% of corrosion class and 1.13% of no corrosion class, respectively. On precision, the MTL-D network outperforms with a 5.92% improvement for the corrosion class and comparable performance of 97.50% for the no corrosion class. On recall, it is observed that an increase (1.33%) and a decrease (1.18%) in no corrosion and corrosion, respectively. This is because corrosion typically occurs on specific bridge elements that are easily contacted by deck runoff and traffic-generated aerosols. The element features offer hints for the corrosion segmentation task.

All in all, the MTL-I model has a much better performance on the bridge element parsing task and comparable performance on the corrosion segmentation task compared with the MTL-D network. It is recommended to use the MTL-I network in the application and implementation.

TABLE 4: Performance comparison by class between single-task and well-performed MTL networks

Class	IoU			Precision			Recall		
	Single	MTL-D	MTL-I	Single	MTL-D	MTL-I	Single	MTL-D	MTL-I
Element									
Bearing	81.00	79.96	81.27	86.09	86.30	88.59	93.20	91.59	90.77
Bracing	72.01	77.32	78.43	85.15	88.65	83.38	82.35	85.82	92.96
Deck	86.03	88.57	91.05	95.31	96.63	96.55	89.83	91.39	94.11
Floor beam	87.60	88.09	88.44	93.48	95.82	97.09	93.30	91.60	90.85
Girder	94.07	94.10	94.65	96.23	96.07	96.68	97.67	97.87	97.83
Substructure	82.41	84.04	85.05	87.31	88.05	89.13	93.62	84.86	94.89
Background	77.10	78.87	79.50	91.67	92.53	92.58	82.91	84.16	84.91
Defect									
Corrosion	68.06	71.84	70.49	76.76	82.68	82.21	85.75	84.57	83.17
No corrosion	93.64	94.77	94.52	97.65	97.50	97.27	95.80	97.13	97.09

The highest values of each metric for each class among all networks are shown in bold

Efficiency

Besides the promising improvement of the MTL models on the task performance metrics, another advantage of MTL over the model composed of two independent single-task networks is the efficiency. TABLE 5 compares the computational time in terms of training time and inference speed between the use of the single-task networks and a MTL network like MTL-D and MTL-I.

The total training time of the two single-task networks was slightly higher than that of the MTL-I network. However, it was almost double of the training time for the MTL-D network. This is because the MTL-D network has quite similar architecture to that of the single-task networks except for an additional segmentation head. The MTL-L has more complex architecture and projection matrix. The MTL models can reduce training time because, instead of investing time training many models on multiple tasks, they only need to train a single model with one or

more model components shared by the multiple tasks. In this study, the two tasks share the feature extractor in a MTL model.

For the inference speed, the two MTL models have similar performance, which is faster than the single-task model. Conducting the forward pass through the encoder is the main computational overhead for the inference. Using the MTL model speeds up the inference due to sharing a feature extractor for all tasks.

TABLE 5: Comparison of Computational Time

Computation time	Single	MTL-D	MTL-I
Training time (min)	26.85	15.93	20.42
Inference speed* (FPS)	11.3	14.6	14.6

* Nvidia Tesla V100 GPU with batch size 1

Besides, the MTL model can provide a preliminary evaluation of bridge elements based on the element parsing and defect segmentation results for the inspector at the same time and in the same model. In this study, the developed MTL model can provide the proportion of corrosion area in each kind of element. The proportion can be an indicator for the inspectors to produce a preliminary condition assessment of bridge elements. It also can be an indicator to selectively apply other high-resolution sensors to areas of developed surface corrosion. Instead, using the two single-task networks needs post-processing for the predictions to produce such an indicator. Therefore, the MTL model is more suitable for deployment on UAV hardware platforms than on single-task networks, which could save the limited computational resource.

Qualitative Examples

FIGURE 3 illustrates two typical example results of automated bridge inspection image analysis using the MTL models and the single-task networks. The MTL models performed better than single-task networks on respective tasks, as evidenced in TABLE 4, because the bridge element parsing task and corrosion segmentation task would cooperate to strengthen the accurate prediction.

For the bridge parsing task, the MTL-I model had a better performance than others. In example (a), the single-task network for element parsing failed to segment the substructure in the distance and part of the bracing elements, and the MTL-I model segmented them successfully. Compared with the MTL-D model, MTL-I has fewer false positives for deck and more true positives for substructure. In example (b), the segmentation results from the single-task network and MTL-D on the floor beam were more incomplete than MTL-I. The MTL-I model also generated more accurate segmentation results on the girder in the dark area of the input image. These observations explained why the MTL-I model obtained the highest precision on floor beam and girder among all networks.

For the corrosion segmentation task, the MTL-D model provides the most accurate segmentation results among all. Specifically, the MTL-D model generates fewer false positives than the single-task network and more true positives than MTL-I on corrosion prediction, which suggests the reason for the highest precision on corrosion by the MTL-D. In example (a), the MTL-D model provides similar segmentation results to the single-task model and MTL-D. In example (b),

the MTL-D model has more accurate predictions on the left bearing. These examples show that the element parsing task and corrosion segmentation benefited from each other on the edge between different classes.

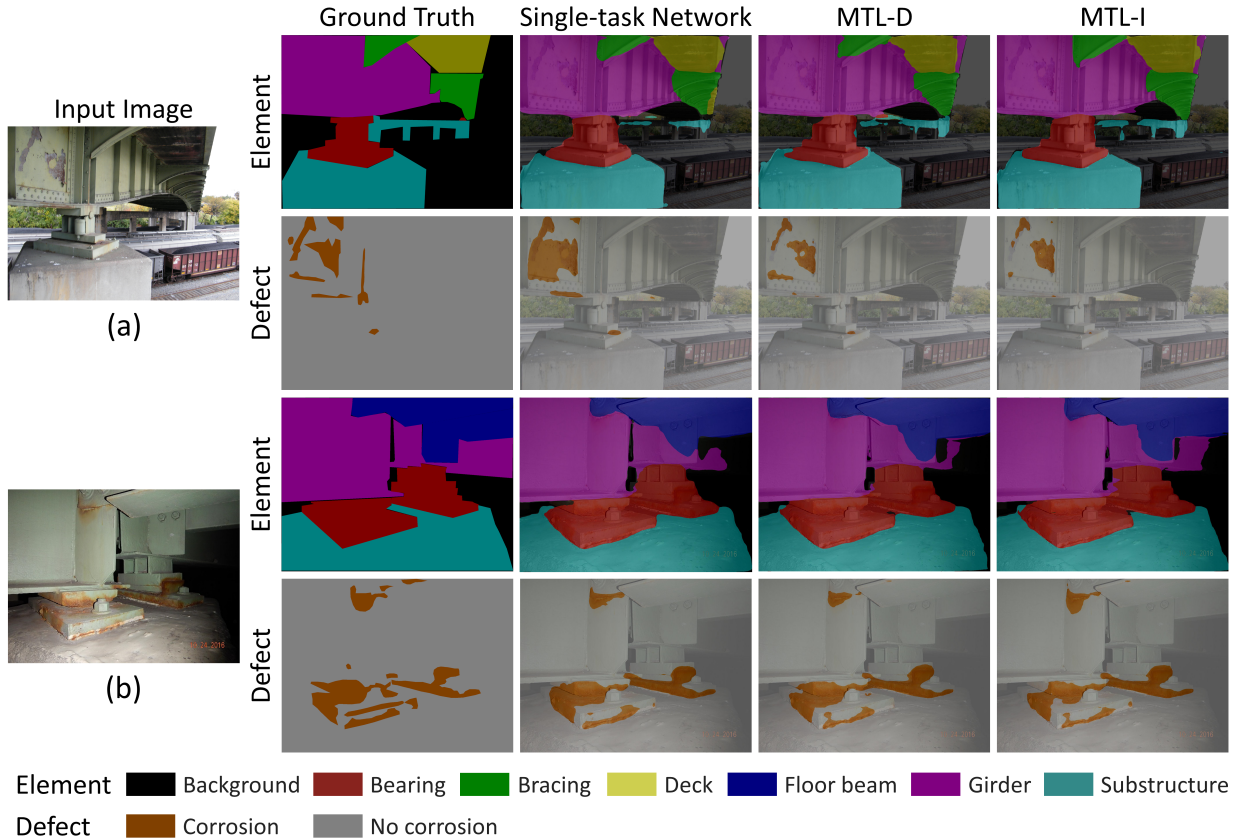


FIGURE 3: Comparison of the Results from Single-task Networks and MTL Networks

CONCLUSIONS

This paper presented a MTL model for parsing bridge elements and simultaneously segmenting defect from bridge inspection images. The proposed network learns common features of both the bridge elements and the surface defect using a shared feature extractor, and then it split into two branches that each is composed of a feature projection and a segmentation network. This study shows that collaborative training of different but related tasks helps boost the performance of the network by learning generalized and contextual information better. The bridge elements and corrosion annotations were developed on bridge inspection images to assess the performance of the proposed network. The effectiveness of the different designs were explored, including the feature projection network, the cross-talk between the network's two branches, and the loss function. The experimental evaluation on the dataset confirms that the proposed MTL model performs better than the single-task networks, with 2.59 % improvement in the mIoU of the element parsing task and 2.46% in the corrosion segmentation task. The proposed MTL model also offers lower computational time with less training time and a faster inference speed. Both the qualitative and quantitative results confirm that the proposed MTL model has multiple advantages over independent single-task

networks. Therefore, the MTL model can be deployed on UAV's hardware platforms to provide the on-site bridge condition evaluation.

This paper has identified room for improvement. For example, modification of the developed model to achieve real-time inference is highly desired for implementation in practice. The inspectors can conduct further inspection instantly at the site using other sensors installed on UAV platforms, like infrared cameras, ultrasonic sensors, and so on, to spy on the potential areas of defective elements found by the RGB-image based model, which avoids the additional time and labor costs. Another important future work is to introduce multiple types of defect not limited to corrosion in the model for a more comprehensive condition assessment of bridge elements. Moreover, the dataset needs to be extended with more images and labels of bridge elements and defects to benefit the broader research community.

AUTHOR CONTRIBUTIONS

The authors confirm contribution to the paper as follows: study conception and design: C. Zhang, M. M. Karim, R. Qin; data collection: C. Zhang; analysis and interpretation of results: C. Zhang, R. Qin; draft manuscript preparation: C. Zhang, M. M. Karim, and R. Qin. All authors reviewed the results and approved the final version of the manuscript.

DECLARATION OF CONFLICTING INTERESTS

The author(s) declared no potential conflicts of interest with respect to the research, authorship, and/or publication of this article.

FUNDING

The author(s) disclosed receipt of the following financial support for the research, authorship, and/or publication of this article: Qin and Karim received support from NSF award ECCS-2026357. Zhang and Karim received support from NSF award ECCS-2025929.

ORCID IDS

Chenyu Zhang: 0000-0003-2500-5070

Muhammad Monjurul Karim: 0000-0002-7830-1407

Ruwen Qin: 0000-0003-2656-8705

References

1. American Road & Transportation Builders Association (ARTBA), *ARTBA Annual Bridge Report*, 2022, <https://artbabridgereport.org>, Accessed August 1, 2022.
2. American Society of Civil Engineers (ASCE), *2021 Report Card for America's Infrastructure*, 2021, <https://infrastructurereportcard.org/cat-item/bridges-infrastructure/>, Accessed August 1, 2022.
3. Federal Highway Administration (FHWA), *National Bridge Inspection Standards*, 2022.
4. Spencer Jr, B. F., V. Hoskere, and Y. Narazaki, Advances in Computer Vision-based Civil Infrastructure Inspection and Monitoring. *Engineering*, Vol. 5, No. 2, 2019, pp. 199–222.
5. American Association of State Highway and Transportation Officials (AASHTO), *Manual for Bridge Element Inspection, 2nd Edition*, 2019.
6. Bianchi, E. and M. Hebdon, Visual Structural Inspection Datasets. *Automation in Construction*, Vol. 139, 2022, p. 104299.
7. Narazaki, Y., V. Hoskere, T. A. Hoang, Y. Fujino, A. Sakurai, and B. F. Spencer Jr, Vision-based Automated Bridge Component Recognition with High-level Scene Consistency. *Computer-Aided Civil and Infrastructure Engineering*, Vol. 35, No. 5, 2020, pp. 465–482.
8. Bianchi, E., A. L. Abbott, P. Tokekar, and M. Hebdon, COCO-Bridge: Structural Detail Data Set for Bridge Inspections. *Journal of Computing in Civil Engineering*, Vol. 35, No. 3, 2021, p. 04021003.
9. Karim, M. M., R. Qin, G. Chen, and Z. Yin, A Semi-supervised Self-training Method to Develop Assistive Intelligence for Segmenting Multiclass Bridge Elements from Inspection Videos. *Structural Health Monitoring*, Vol. 21, No. 3, 2022, pp. 835–852.
10. Zhang, C., M. M. Karim, and R. Qin, A Deep Neural Network for Multiclass Bridge Element Parsing in Inspection Image Analysis. In *Proceedings of the 8th World Conference on Structural Control and Monitoring*, 2022.
11. Zhang, L., F. Yang, Y. D. Zhang, and Y. J. Zhu, Road Crack Detection Using Deep Convolutional Neural Network. In *2016 IEEE International Conference on Image Processing*, IEEE, 2016, pp. 3708–3712.
12. Wang, J., K. Sun, T. Cheng, B. Jiang, C. Deng, Y. Zhao, D. Liu, Y. Mu, M. Tan, X. Wang, et al., Deep High-resolution Representation Learning for Visual Recognition. *IEEE Transactions on Pattern Analysis and Machine Intelligence*, Vol. 43, No. 10, 2020, pp. 3349–3364.
13. Yudin, D. A., V. Adeshkin, A. V. Dolzhenko, A. Polyakov, and A. E. Naumov, Roof Defect Segmentation on Aerial Images Using Neural Networks. In *International Conference on Neuroinformatics*, Springer, 2020, pp. 175–183.
14. Jia, B., X. Luo, R. Tao, and Y. Shi, Surface Defect Detection of Aluminum Material Based on HRNet Feature Extraction. In *2021 4th International Conference on Data Science and Information Technology*, 2021, pp. 44–48.
15. Akhyar, F., C.-Y. Lin, and G. S. Kathiresan, A Beneficial Dual Transformation Approach for Deep Learning Networks Used in Steel Surface Defect Detection. In *Proceedings of the 2021 International Conference on Multimedia Retrieval*, 2021, pp. 619–622.
16. Rubio, J. J., T. Kashiwa, T. Laiteerapong, W. Deng, K. Nagai, S. Escalera, K. Nakayama, Y. Matsuo, and H. Prendinger, Multi-class Structural Damage Segmentation Using Fully Convolutional Networks. *Computers in Industry*, Vol. 112, 2019, p. 103121.

17. Dung, C. V. et al., Autonomous Concrete Crack Detection Using Deep Fully Convolutional Neural Network. *Automation in Construction*, Vol. 99, 2019, pp. 52–58.
18. Ronneberger, O., P. Fischer, and T. Brox, U-net: Convolutional Networks for Biomedical Image Segmentation. In *International Conference on Medical Image Computing and Computer-assisted Intervention*, Springer, 2015, pp. 234–241.
19. Pan, G., Y. Zheng, S. Guo, and Y. Lv, Automatic Sewer Pipe Defect Semantic Segmentation Based on Improved U-Net. *Automation in Construction*, Vol. 119, 2020, p. 103383.
20. Wang, M. and J. C. Cheng, A Unified Convolutional Neural Network Integrated with Conditional Random Field for Pipe Defect Segmentation. *Computer-Aided Civil and Infrastructure Engineering*, Vol. 35, No. 2, 2020, pp. 162–177.
21. Zhao, H., J. Shi, X. Qi, X. Wang, and J. Jia, Pyramid Scene Parsing Network. In *Proceedings of the IEEE Conference on Computer Vision and Pattern Recognition*, 2017, pp. 2881–2890.
22. Shi, J., J. Dang, M. Cui, R. Zuo, K. Shimizu, A. Tsunoda, and Y. Suzuki, Improvement of Damage Segmentation Based on Pixel-level Data Balance Using VGG-Unet. *Applied Sciences*, Vol. 11, No. 2, 2021, p. 518.
23. Ayele, Y. Z., M. Aliyari, D. Griffiths, and E. L. Drogue, Automatic Crack Segmentation for UAV-assisted Bridge Inspection. *Energies*, Vol. 13, No. 23, 2020, p. 6250.
24. Li, J., Q. Wang, J. Ma, and J. Guo, Multi-defect Segmentation from Façade Images Using Balanced Copy-paste Method. *Computer-Aided Civil and Infrastructure Engineering*, 2022.
25. Huang, H., S. Zhao, D. Zhang, and J. Chen, Deep Learning-based Instance Segmentation of Cracks from Shield Tunnel Lining Images. *Structure and Infrastructure Engineering*, Vol. 18, No. 2, 2022, pp. 183–196.
26. Yeum, C. M., J. Choi, and S. J. Dyke, Automated Region-of-interest Localization and Classification for Vision-based Visual Assessment of Civil Infrastructure. *Structural Health Monitoring*, Vol. 18, No. 3, 2019, pp. 675–689.
27. Liu, W., D. Anguelov, D. Erhan, C. Szegedy, S. Reed, C.-Y. Fu, and A. C. Berg, SSD: Single Shot Multibox Detector. In *European Conference on Computer Vision*, Springer, 2016, pp. 21–37.
28. Eigen, D. and R. Fergus, Predicting Depth, Surface Normals and Semantic Labels with a Common Multi-scale Convolutional Architecture. In *Proceedings of the IEEE International Conference on Computer Vision*, 2015, pp. 2650–2658.
29. Bischke, B., P. Helber, J. Folz, D. Borth, and A. Dengel, Multi-task Learning for Segmentation of Building Footprints with Deep Neural Networks. In *2019 IEEE International Conference on Image Processing*, IEEE, 2019, pp. 1480–1484.
30. Tian, Y., P. Luo, X. Wang, and X. Tang, Pedestrian Detection Aided by Deep Learning Semantic Tasks. In *Proceedings of the IEEE Conference on Computer Vision and Pattern Recognition*, 2015, pp. 5079–5087.
31. Zhang, Z., P. Luo, C. C. Loy, and X. Tang, Facial Landmark Detection by Deep Multi-task Learning. In *European Conference on Computer Vision*, Springer, 2014, pp. 94–108.
32. Ruder, S., An Overview of Multi-task Learning in Deep Neural Networks. *arXiv preprint arXiv:1706.05098*, 2017.
33. Zhang, Y. and Q. Yang, A Survey on Multi-task Learning. *IEEE Transactions on Knowledge and Data Engineering*, 2021.

34. Hoskere, V., Y. Narazaki, T. A. Hoang, and B. Spencer Jr, MaDnet: Multi-task Semantic Segmentation of Multiple Types of Structural Materials and Damage in Images of Civil Infrastructure. *Journal of Civil Structural Health Monitoring*, Vol. 10, No. 5, 2020, pp. 757–773.
35. Gong, T., T. Lee, C. Stephenson, V. Renduchintala, S. Padhy, A. Ndirango, G. Keskin, and O. H. Elibol, A Comparison of Loss Weighting Strategies for Multi Task Learning in Deep Neural Networks. *IEEE Access*, Vol. 7, 2019, pp. 141627–141632.
36. Kendall, A., Y. Gal, and R. Cipolla, Multi-task Learning Using Uncertainty to Weigh Losses for Scene Geometry and Semantics. In *Proceedings of the IEEE Conference on Computer Vision and Pattern Recognition*, 2018, pp. 7482–7491.
37. Bianchi, E. and M. Hebdon, *Corrosion Condition State Semantic Segmentation Dataset*, 2021.
38. Russell, B. C., A. Torralba, K. P. Murphy, and W. T. Freeman, LabelMe: a Database and Web-based Tool for Image Annotation. *International Journal of Computer Vision*, Vol. 77, No. 1, 2008, pp. 157–173.